

Decay dynamics of nascent acetonitrile and nitromethane dipole-bound anions produced by intracluster charge-transfer

Margaret A. Yandell, Sarah B. King, and Daniel M. Neumark

Citation: *The Journal of Chemical Physics* **140**, 184317 (2014); doi: 10.1063/1.4875021

View online: <http://dx.doi.org/10.1063/1.4875021>

View Table of Contents: <http://scitation.aip.org/content/aip/journal/jcp/140/18?ver=pdfcov>

Published by the [AIP Publishing](#)

Articles you may be interested in

Low-energy photoelectron imaging spectroscopy of nitromethane anions: Electron affinity, vibrational features, anisotropies, and the dipole-bound state

J. Chem. Phys. **130**, 074307 (2009); 10.1063/1.3076892

Vibronic Spectra of Mixed Frenkel and Charge Transfer Excitons

AIP Conf. Proc. **899**, 57 (2007); 10.1063/1.2733042

Preparation and photoelectron spectrum of the glycine molecular anion: Assignment to a dipole-bound electron species with a high-dipole moment, non-zwitterionic form of the neutral core

J. Chem. Phys. **120**, 9899 (2004); 10.1063/1.1755196

Femtosecond dynamics of solvated oxygen anions. I. Bifurcated electron transfer dynamics probed by photoelectron spectroscopy

J. Chem. Phys. **118**, 6923 (2003); 10.1063/1.1561433

Femtochemistry of mass-selected negative-ion clusters of dioxygen: Charge-transfer and solvation dynamics

J. Chem. Phys. **115**, 612 (2001); 10.1063/1.1384549

A row of several tablets or small monitors displaying the cover of the journal 'Computing: Science & Engineering'. The covers feature a colorful, abstract, circular pattern. The text 'Computing' is at the top, and 'SCIENCE & ENGINEERING' is below it. At the bottom of the covers, the text 'A JOURNAL OF COMPUTATIONAL TOOLS AND METHODS' is visible. In the bottom right corner of the image, the journal's logo 'computing SCIENCE & ENGINEERING' is displayed. Below the image, the text 'AIP'S JOURNAL OF COMPUTATIONAL TOOLS AND METHODS. AVAILABLE AT MOST LIBRARIES.' is written in large, white, bold letters.

Decay dynamics of nascent acetonitrile and nitromethane dipole-bound anions produced by intracuster charge-transfer

Margaret A. Yandell,¹ Sarah B. King,¹ and Daniel M. Neumark^{1,2,a)}

¹Department of Chemistry, University of California, Berkeley, California 94720, USA

²Chemical Sciences Division, Lawrence Berkeley National Laboratory, Berkeley, California 94720, USA

(Received 19 March 2014; accepted 24 April 2014; published online 13 May 2014)

Decay dynamics of nascent dipole bound states of acetonitrile and nitromethane are examined using time-resolved photoelectron imaging of iodide-acetonitrile ($I^- \cdot CH_3CN$) and iodide-nitromethane ($I^- \cdot CH_3NO_2$) complexes. Dipole-bound anions are created by UV-initiated electron transfer to the molecule of interest from the associated iodide ion at energies just below the vertical detachment energy of the halide-molecule complex. The acetonitrile anion is observed to decay biexponentially with time constants in the range of 4–900 ps. In contrast, the dipole bound state of nitromethane decays rapidly over 400 fs to form the valence bound anion. The nitromethane valence anion species then decays biexponentially with time constants of 2 ps and 1200 ps. The biexponential decay dynamics in acetonitrile are interpreted as iodine atom loss and autodetachment from the excited dipole-bound anion, followed by slower autodetachment of the relaxed metastable ion, while the dynamics of the nitromethane system suggest that a dipole-bound anion to valence anion transition proceeds via intramolecular vibrational energy redistribution to nitro group modes in the vicinity of the iodine atom. © 2014 AIP Publishing LLC. [<http://dx.doi.org/10.1063/1.4875021>]

I. INTRODUCTION

In recent decades, much theoretical and experimental work has focused on the study of dipole-bound anions. Fermi and Teller predicted that fixed dipoles with dipole moments μ greater than 1.6 D should bind electrons via dipolar ($-1/r^2$) interactions,^{1,2} while Crawford and Garrett later determined that rotating molecules in the gas phase with dipole moments greater than 2 D should stably bind electrons in diffuse orbitals with low electron affinities (10 s of meV).^{3–7} Polar species such as acetonitrile (CH_3CN),^{8,9} the water dimer,¹⁰ the nucleobases uracil and thymine,¹¹ and small ketones and aldehydes¹² have been observed to form ground-state dipole-bound anions. Dipole-bound states (DBSs) have also been detected as excited electronic states or vibrational Feshbach resonances of conventional valence anions in cyanomethide¹³ and other species.^{14,15} In nitromethane (CH_3NO_2), the DBS of the anion has been described as a “doorway” to a more stable valence-bound state (VBS), with the DBS to VBS transition occurring on a timescale competitive with electron autodetachment.^{16–18} In this study, we carry out time-resolved photoelectron imaging on $I^- \cdot CH_3CN$ and $I^- \cdot CH_3NO_2$ binary complexes to directly observe the formation and lifetimes of the dipole-bound anions of acetonitrile and nitromethane as well as the DBS to VBS transition in $CH_3NO_2^-$.

The dipole-bound ground state of CH_3CN^- was one of the first such species to be examined.^{8,9,19} The diffuse orbital bearing the excess electron is supported at the electropositive methyl end of acetonitrile by a large dipole moment

($\mu = 3.92$ D) and minimally distorts the geometry of the molecule from that of the neutral.^{20,21} Acetonitrile anion formation via Rydberg electron transfer (RET) collisions with Xe atoms in highly excited Rydberg states occurs most efficiently for atoms with principal quantum numbers near $n = 13$,^{22,23} while field detachment of these species estimated an electron binding energy (eBE) of approximately 11 meV,^{22,24} characteristic of diffuse dipole-bound states. In experiments by Johnson and co-workers,²⁵ CH_3CN^- was produced by photo-induced intracomplex charge transfer in $I^- \cdot CH_3CN$ near 3.54 eV, the peak of the photoelectron spectrum (the vertical detachment energy, VDE) of the complex. This species was identified as a dipole-bound state via its photoelectron spectrum, which displayed a single narrow peak with an eBE of about 10 meV. The lifetimes of weakly excited dipole-bound anions of acetonitrile generated by RET have been observed to exceed microseconds,^{26–28} with electron autodetachment²² or black-body induced photodetachment^{26–28} identified as the primary decay mechanisms for the metastable species. No acetonitrile valence anion is expected to exist as the lowest unoccupied molecular orbital occurs nearly 3 eV above the neutral ground state.^{29,30}

Formation of the nitromethane anion, $CH_3NO_2^-$, has been observed upon RET from rare gas⁸ and alkali atoms¹⁶ to CH_3NO_2 and in collisions of CH_3NO_2 with high energy alkali atoms.^{31,32} The anion has been investigated by PES,^{16,33,34} and its vibrational spectrum has been measured via autodetachment spectroscopy.^{35,36} Nitromethane has a dipole moment of 3.46 D, which is sufficient to support a dipole-bound anion. However, RET experiments show that the range of Rydberg states over which electron transfer to CH_3NO_2 occurs is considerably broader than that observed when a pure DBS state is formed (i.e., in CH_3CN), implying coupling between

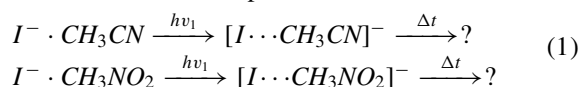
^{a)} Author to whom correspondence should be addressed. Electronic mail: dneumark@berkeley.edu.

the nitromethane anion DBS and the more strongly bound VBS.¹⁶ Indeed, the negative ion photoelectron spectrum of nitromethane anions produced in a supersonic expansion of seeded argon gas reported in the same paper was quite broad, with extensive, partially resolved vibrational structure and a VDE of ~ 1 eV. Such a spectrum is characteristic of a valence anion with a geometry differing from that of the neutral species, as opposed to the dominance of the vibrational origin typically seen at very low eBE in the photoelectron spectrum of a dipole-bound anion.

The photoelectron spectrum of CH_3NO_2^- measured by Weber and co-workers³⁴ shows features attributable to both the DB and VB anions with adiabatic detachment energies of 8 and 172 meV, respectively, placing the VBS 164 meV below the DBS. The absence of the DBS signature in other PE spectra^{16,33} and the suppression of the DBS in RET to CH_3NO_2 complexed to a single Ar atom²³ suggest that the dipole-bound anion of nitromethane is a fragile species formed only under restricted conditions, consistent with the picture of a low-energy curve crossing with the VBS.¹⁷ The experimental evidence suggestive of a DBS to VBS transition for the nitromethane anion is in accordance with electronic structure calculations that show the VBS to be more stable than the DBS.^{37,38}

The $\text{I}^- \cdot \text{CH}_3\text{NO}_2$ complex studied here has previously been investigated by photofragment action spectroscopy³⁹ and photoelectron imaging.⁴⁰ The action spectroscopy experiments, in which anionic and neutral fragments were detected as functions of excitation energy, yielded an electronic absorption spectrum of the complex peaking just below 3.60 eV, the VDE of the initial complex. The electronic band was attributed to a dipole-bound excited state of the complex, which was observed to decay to CH_3NO_2^- as well as I^- and NO_2^- . The CH_3NO_2^- photofragment was characterized by electric field stripping experiments which, by comparison with similar experiments on anions formed via RET,¹⁶ suggested that the photofragment anion exhibited some DBS character. The authors attributed vibrational resonances measured in the action spectra of the other photofragments to nitro-associated modes relevant to the valence anion, providing further evidence for mixing of the DBS and VBS states.

In this work, we examine the nature and decay dynamics of acetonitrile and nitromethane anions produced upon photoexcitation of binary iodide-molecule complexes using time-resolved photoelectron spectroscopy (TRPES). These experiments represent a continuation of efforts in which TRPES is used to study electron-induced cluster dynamics promoted by photodetachment of a complexed iodide anion.^{41,42} In analogy to our earlier work with iodide-nucleobase complexes^{43,44} and the work of others,^{25,39} transient negative ions (TNIs) of the form $[\text{I} \cdots \text{M}]^-$ are generated via photo-initiated charge transfer from iodide to the associated molecule by a femtosecond UV pulse $h\nu_1$ with energy near the VDE of the complex:



The dynamics of the TNIs are monitored by photodetachment with a femtosecond near-IR probe pulse $h\nu_2$ by

recording electron kinetic energy (eKE) and photoelectron angular distributions (PADs) of the resultant electrons using photoelectron imaging. The acetonitrile anion is formed in and remains a DBS, decaying via autodetachment and iodine atom loss over hundreds of picoseconds, while the nitromethane anion is initially formed in a DBS but decays within hundreds of femtoseconds to form the VBS. The resulting vibrationally excited VBS exhibits biexponential decay with time constants of 2 ps and 1200 ps that are attributed to decay via autodetachment and iodine atom loss. This study provides further insight into the decay mechanisms of biologically relevant systems such as pyrimidine nucleobase anions that also exist as both dipole- and valence-bound states.^{11,45,46}

II. EXPERIMENTAL METHODS

The $\text{I}^- \cdot \text{CH}_3\text{CN}$ and $\text{I}^- \cdot \text{CH}_3\text{NO}_2$ complexes were studied using femtosecond time-resolved photoelectron imaging. Detailed descriptions of the imaging apparatus and laser system have been presented in Refs. 47–49. Binary complexes were created by flowing 50 psig of neon gas over a supply of iodomethane and a reservoir of the liquid of interest chilled with ice water. The gaseous mixture was subsequently expanded through an Even-Lavie valve⁵⁰ pulsed at 500 Hz and crossed with a ring electrode ionizer to create halide-molecule cluster anions. The anionic clusters were then perpendicularly extracted with a Wiley-McLaren time-of-flight mass spectrometer⁵¹ and steered with ion optics toward a mass gate for isolation of the relevant species.

The ultraviolet pump pulse was generated from a 1 kHz, 1.6 mJ near-IR pulse (KM Labs Griffin Oscillator and Dragon Amplifier) by frequency doubling the second harmonic signal of an optical parametric amplifier (Light Conversion TOPAS-C). Pump photon energies were selected based on the relative photoabsorption cross sections reported by Johnson and co-workers.^{25,39} Most data were taken at two excitation energies for each system: one resonant with the maximum absorption (3.53 eV and 3.60 eV for the acetonitrile and nitromethane systems, respectively) and other slightly off-resonant (3.47 eV and 3.53 eV, respectively). The fundamental at 1.56 eV was used as the probe. Cross correlations measured outside the chamber yielded values below 150 fs.

Photoelectrons were directed toward a chevron-stacked pair of microchannel plates coupled to a phosphor screen using a 3-plate velocity map imaging ion optical assembly. 2D photoelectron distributions were imaged using a charge-coupled device camera; from these images, 3D photoelectron kinetic energy (eKE) distributions and photoelectron angular distributions (PADs) were reconstructed using the basis-set expansion (BASEX)⁵² and polar onion peeling (POP)⁵³ methods. The BASEX method produces more reliable eKE distributions near zero eKE (corresponding to the image center) than POP, for which center-point noise obscures photoelectron signal in this energy region. However, PADs obtained from BASEX reconstruction suffer from more noise away from the image center than those obtained with POP. Thus, eKE distributions were examined with BASEX, while PADs were examined with POP.

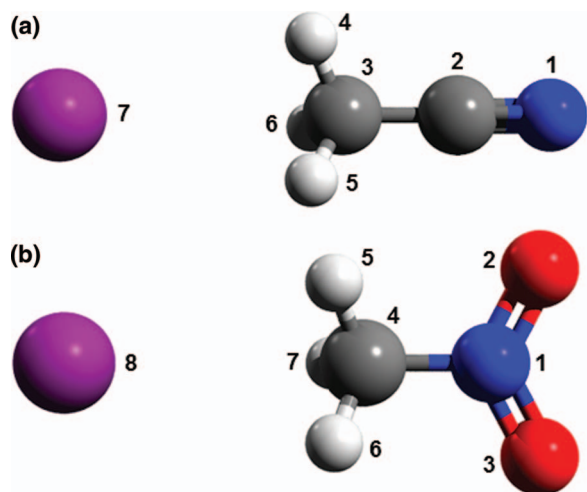


FIG. 1. Optimized structures for the (a) $I^- \cdot CH_3CN$ and (b) $I^- \cdot CH_3NO_2$ complexes. Calculations were performed at the MP2/aug-cc-pVDZ level using the aug-cc-pVDZ pseudopotential for iodide. Relevant parameters are listed in Table I.

Anisotropy parameters, β_i , were extracted by fitting the photoelectron angular distributions according to⁵⁴

$$I(\theta) = \frac{\sigma_{total}}{4\pi} [1 + \beta_2 P_2(\cos \theta) + \beta_4 P_4(\cos \theta)], \quad (2)$$

in which σ_{total} represents the total photodetachment cross section, θ is the angle between the laser polarization and the ejected electron, and P_i is a Legendre polynomial. β_2 is constrained to values between -1 and 2 , corresponding to perpendicular and parallel detachment processes, respectively. Single-photon processes should show no dependence on β_4 .

III. THEORETICAL METHODS

Geometry optimizations of the binary anion complexes were performed using the Gaussian 09⁵⁵ computational suite at the MP2/aug-cc-pVDZ level with an aug-cc-pVDZ pseudopotential⁵⁶ for iodide. Optimized structures of the $I^- \cdot CH_3CN$ and $I^- \cdot CH_3NO_2$ complexes are presented in

Figure 1, while relevant bond distances and other parameters are summarized in Table I. Previously calculated^{20,21} parameters for the acetonitrile DB anion, the nitromethane VB anion, and both bare neutral species are also included. The linear alignment of the iodide with the methyl end of the acetonitrile molecule is consistent with previously calculated structures.^{57–59} The iodide is situated 3.61 \AA from the methyl carbon atom and minimally perturbs the structure of the molecule.²¹ In the nitromethane system, the iodide sits slightly closer and non-collinearly to the molecular axis and interacts more strongly with the methyl group, noticeably reorienting two of the hydrogen atoms. The plane containing the nitro group is also slightly tilted relative to this axis in both $I^- \cdot CH_3NO_2$ and neutral CH_3NO_2 and is significantly distorted in the nitromethane valence anion.³⁷ VDEs for $I^- \cdot CH_3CN$ and $I^- \cdot CH_3NO_2$ were calculated to be 3.55 and 3.62 eV , in good agreement with experimental values.^{25,39}

IV. RESULTS

A. Iodide-acetonitrile

Time-resolved photoelectron images for $I^- \cdot CH_3CN$ were recorded at excitation energies ranging from 3.43 eV to 3.59 eV . Representative POP-reconstructed Cartesian images measured at three pump-probe delays using a pump photon energy of 3.47 eV are displayed in Figure 2(a). At negative pump-probe delays, where the 1.56 eV probe pulse arrives prior to the UV pump pulse, we observe an intense, isotropic feature A at the image center, corresponding to near-zero electron kinetic energy. At $\Delta t = 0$, two additional features B and C appear. Both features display anisotropy, showing greater intensity at approximately $\theta = \frac{\pi}{4}$. At $\Delta t = 267 \text{ fs}$, feature B is no longer apparent, and the photoelectron angular distribution of feature C is most intense at $\theta = 0$, suggestive of parallel detachment.

Figure 3(a) shows a contour plot of eKE distributions for the iodide-acetonitrile complex over a range of pump-probe delays. Feature A is several orders of magnitude more

TABLE I. Relevant structural parameters for the $I^- \cdot CH_3CN$ and $I^- \cdot CH_3NO_2$ complexes and the respective bare neutral and valence anion species. Bond distances are presented in angstroms, angles in degrees, and dipole moments in debyes. The value α is the angle between the C—H bond and the C—C bond axis in CH_3CN , while θ_{tilt} is the angle between the plane containing the nitro group and the C—N bond axis of CH_3NO_2 .

	CH_3CN^a	CH_3CN^{-a}	$I^- \cdot CH_3CN$		$CH_3NO_2^b$	$CH_3NO_2^{-b}$	$I^- \cdot CH_3NO_2$
R(C—N)	1.185	1.186	1.187	R(C—N)	1.493	1.462	1.496
R(C—C)	1.471	1.471	1.472	R(C—H ₇)	1.086	1.099	1.097
R(C—H)	1.099	1.099	1.098	R(C—H _{5,6})	1.082	1.088	1.093
R(C—I)			3.609	R(N—O)	1.229	1.314	1.242
α	109.8	109.9	111.2	R(C—I)			3.511
				$\angle NCI$			178.1
				$\angle NCH_{5,6}$	107.92	109.06	108.7
				$\angle H_5CH_6$	118.9	119.72	112.5
				$\angle NCH_1$	106.78	108.93	107.7
				$\angle CNO$	117.09	113.64	118
				θ_{tilt}	1.53	33.73	1.80

^aReference 21.

^bReference 20.

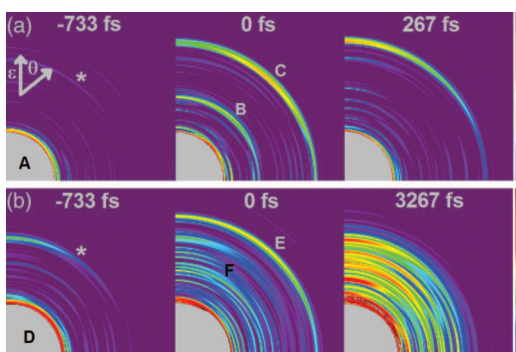


FIG. 2. Representative POP-reconstructed Cartesian photoelectron images for (a) $\text{I}^- \cdot \text{CH}_3\text{CN}$ excited at 3.47 eV and (b) $\text{I}^- \cdot \text{CH}_3\text{NO}_2$ excited at 3.60 eV. Both systems are probed at 1.56 eV. As images are four-way symmetrized for analysis, only a single quadrant is displayed. The laser polarization is indicated to be vertical. The grey spot in the center of each image represents near-zero kinetic energy electrons, which are several orders of magnitude more intense than transient photoelectron signals. The starred features correspond to three-photon detachment of the initial complex by the probe pulse.

intense than the other features and shows no notable intensity variation with pump-probe delay, so it is largely excluded for clarity. The weak feature at 1.1 eV, which corresponds to the starred feature at negative time delays in Figure 2(a), shows minimal time variation and is assigned as three-probe-photon detachment of $\text{I}^- \cdot \text{CH}_3\text{CN}$. Feature B rapidly appears and disappears around $\Delta t = 0$. Its eKE of ~ 0.6 eV corresponds to an electron binding energy, eBE, of 0.96 eV ($\text{eBE} = h\nu - \text{eKE}$). Feature C emerges at $\Delta t = 0$ and undergoes a large decrease in intensity as well as a small change in eKE over 1 ps, eventually settling at 1.54 eV and persisting for hundreds of ps. Both features B and C are relatively narrow, displaying widths limited by the energy resolution of the femtosecond photoelectron spectrometer (~ 50 meV).

Figure 4(a) displays the integrated intensities of the transient features B and C at short pump-probe delays. Feature B peaks at $\Delta t = 0$ and then disappears, while feature C is markedly different near and away from $\Delta t = 0$, mimicking feature B around $\Delta t = 0$ and then dropping in intensity to a slowly decaying signal. Accordingly, feature C is best described as consisting of two components, C_1 and C_2 , at early ($\Delta t < 120$ fs) and later delays, respectively, as delineated in Figure 4(a). The intensity of feature C_2 decays to approximately half of its initial intensity by 1 ns, the longest pump-probe delay sampled (Figure 4(b)). Figure 5 shows that the relative integrated intensities of features C_1 and C_2 vary significantly with excitation energy, with the highest value C_2/C_1 seen at 3.53 eV (green triangles), closest to the peak in the electronic absorption spectrum.²⁵ As shown in Figure 6, over the range of pump energies used here, the central eKE observed for feature C_2 remains static, while that for C_1 shifts to higher eKE as the pump energy is increased.

The anisotropy parameters associated with feature C for $\text{I}^- \cdot \text{CH}_3\text{CN}$ excited at 3.47 eV are shown in Figure 7(a), superimposed upon the integrated intensity of the feature. At $\Delta t = 0$, where feature C_1 dominates, β_2 is approximately 0.3 while β_4 is -0.6 . These values increase to asymptotic values near 0.9 and 0, respectively, for feature C_2 . Anisotropy

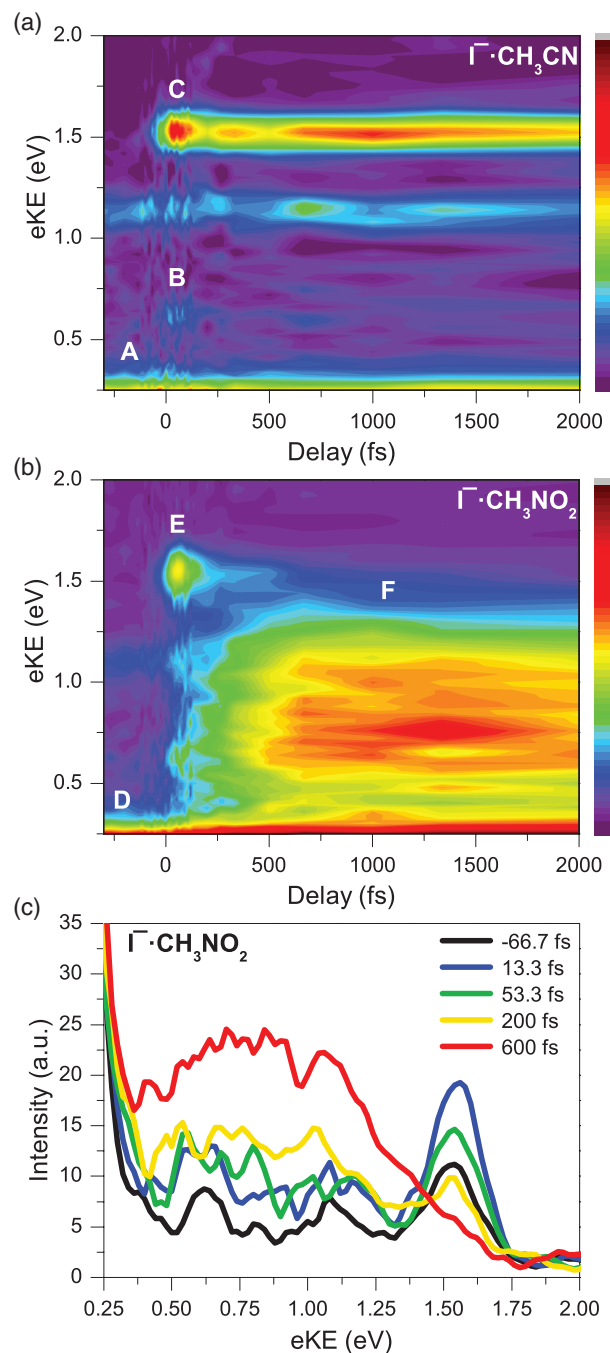


FIG. 3. Time-resolved photoelectron (TRPE) spectra at short pump-probe delays for (a) $\text{I}^- \cdot \text{CH}_3\text{CN}$ excited at 3.55 eV and (b) $\text{I}^- \cdot \text{CH}_3\text{NO}_2$ excited at 3.60 eV. Panel (c) shows photoelectron spectra at selected delays for $\text{I}^- \cdot \text{CH}_3\text{NO}_2$. Both systems were probed at 1.56 eV.

parameters do not exhibit any notable changes with excitation energy.

B. Iodide-nitromethane

Representative photoelectron images for $\text{I}^- \cdot \text{CH}_3\text{NO}_2$ excited at 3.60 eV are displayed in Figure 2(b). As observed for $\text{I}^- \cdot \text{CH}_3\text{CN}$, at negative delays, the images are dominated by a central isotropic feature (D). The additional weak feature at larger eKE indicated with a star is barely apparent at later times and is attributable to three-photon detachment of

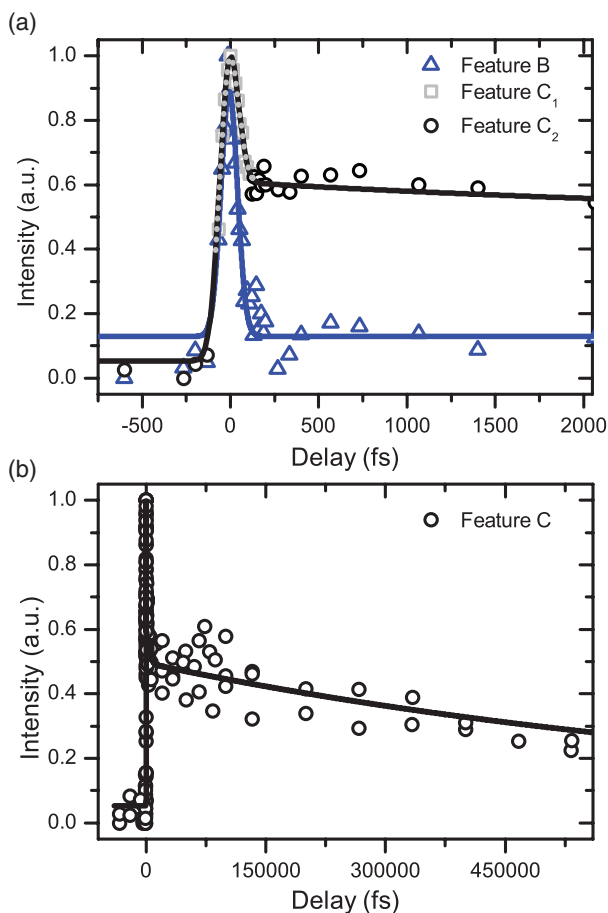


FIG. 4. Integrated intensities of the transient features observed in $\text{I}^- \cdot \text{CH}_3\text{CN}$ TRPE spectra pumped with 3.47 eV and probed at 1.56 eV. Panel (a) shows the early decay dynamics of features C_1 (gray squares) and C_2 (black circles) and the cross-correlation limited feature B (blue triangles), while panel (b) shows the long-time decay of feature C. Fits are displayed as solid lines.

$\text{I}^- \cdot \text{CH}_3\text{NO}_2$ by the probe pulse. The image at $\Delta t = 0$ includes a well-defined anisotropic feature E similar to feature C observed for the $\text{I}^- \cdot \text{CH}_3\text{CN}$ system. In addition to this feature, a low intensity, weakly anisotropic feature F spans eKEs between features D and E. In the last image, at $\Delta t = 3267$ fs, feature E has disappeared and the intensity of feature F has significantly increased.

Figure 3(b) displays eKE distributions for $\text{I}^- \cdot \text{CH}_3\text{NO}_2$ over a range of pump-probe delays. Like feature A observed for $\text{I}^- \cdot \text{CH}_3\text{CN}$, the largely excluded feature D at low eKE dominates the time-resolved photoelectron spectra and varies minimally with pump-probe delay. The narrow feature E at 1.54 eV shows no variation in eKE with excitation energy and decays rapidly after $\Delta t = 0$. The decay of feature E precedes the rise of the more intense feature F, an uneven and broad feature that spans the energy range 0.3–1.5 eV. The intensity of feature F achieves a maximum after approximately 1 ps and then decreases slowly over hundreds of ps. Photoelectron spectra at selected short pump-probe delays are presented in Figure 3(c). The spectra emphasize the apparent intensity exchange between features E and F and their distinct spectral signatures. Some overlap between features E and F occurs in the range of 1.4 eV.

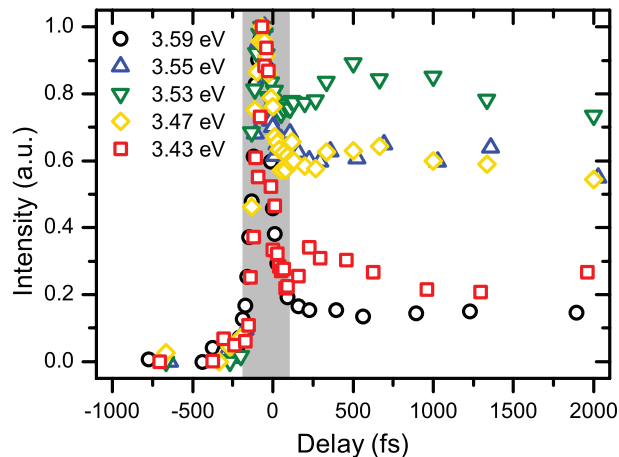


FIG. 5. Comparison of integrated intensities of the transient feature C illustrating the variance in the relative intensities of features C_1 (gray background) and C_2 (white background) observed in $\text{I}^- \cdot \text{CH}_3\text{CN}$ TRPE spectra measured with a range of pump energies and probed at 1.56 eV.

The integrated intensities of features E and F are presented in Figure 8. Feature E exhibits fast decay over hundreds of fs while feature F displays a near-complementary rise, peaking at about 1 ps before decaying biexponentially (see Sec. V) over hundreds of ps. Time-dependent anisotropy parameters β_2 and β_4 are superimposed on the integrated intensities of features E and F in Figures 7(b) and 7(c). β_2 for both features shows minimal variation with pump-probe delay and maintains a value near 0.6. Some variation in β_4 is apparent near $\Delta t = 0$ for both features, with the value increasing from slightly negative values to approximately 0 within 200 fs.

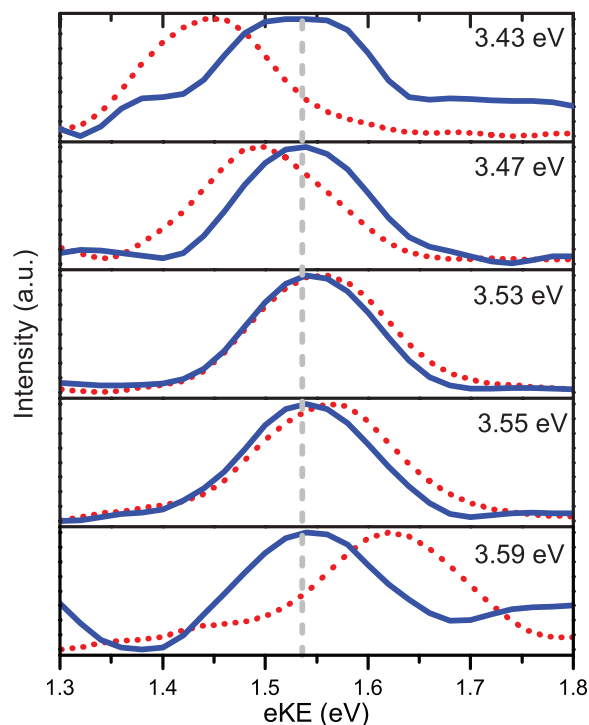


FIG. 6. Comparison of electron kinetic energies (eKEs) of features C_1 (red dotted lines) and C_2 (blue lines) of $\text{I}^- \cdot \text{CH}_3\text{CN}$ measured with several different excitation energies. The gray dashed line denotes 1.54 eV, the peak eKE value for C_2 with all excitation energies.

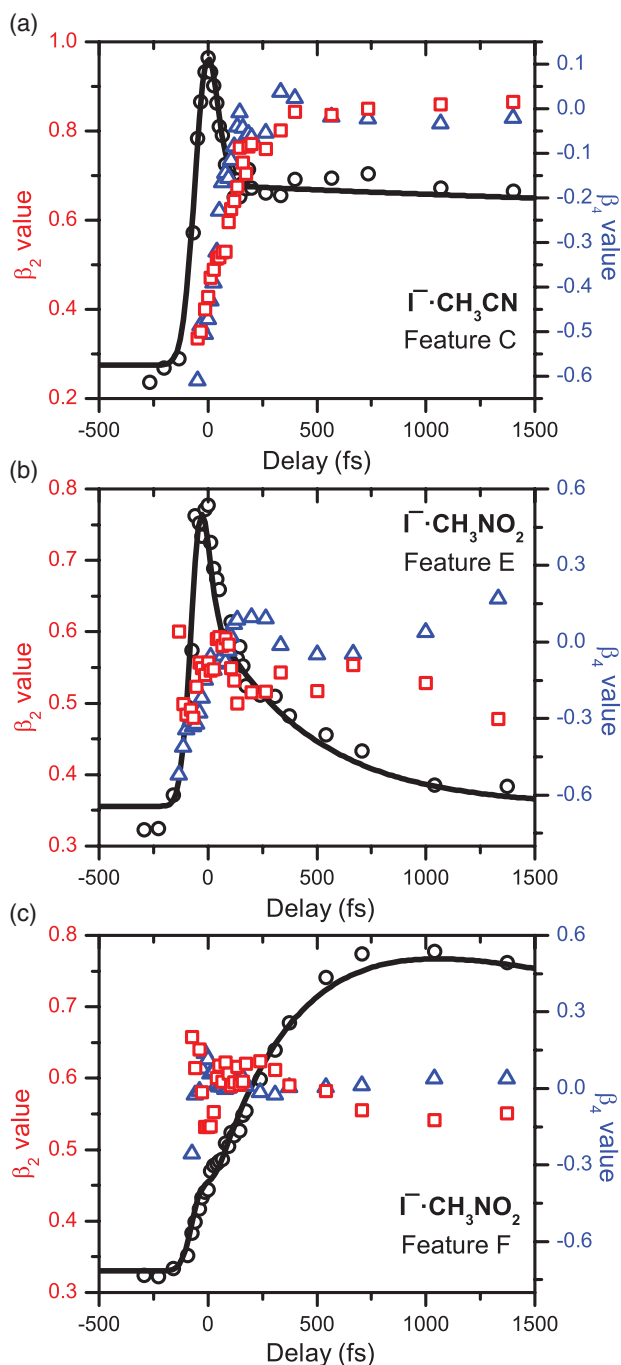


FIG. 7. Anisotropy parameters associated with the (a) transient feature C observed in $\Gamma^- \cdot \text{CH}_3\text{CN}$ TRPE spectra excited at 3.47 eV and the transient features (b) E and (c) F observed in $\Gamma^- \cdot \text{CH}_3\text{NO}_2$ TRPE spectra excited at 3.60 eV. Both systems were probed at 1.56 eV. Representative β_2 (red squares) and β_4 values (blue triangles) are shown against the integrated intensities (black circles) of the features.

V. ANALYSIS

The time evolution of the transient features observed can be described by a convolution of a Gaussian laser response function

$$L(t) = \frac{1}{\sigma_{CC}\sqrt{2\pi}} \exp\left(\frac{-t^2}{2\sigma_{CC}^2}\right) \quad (3)$$

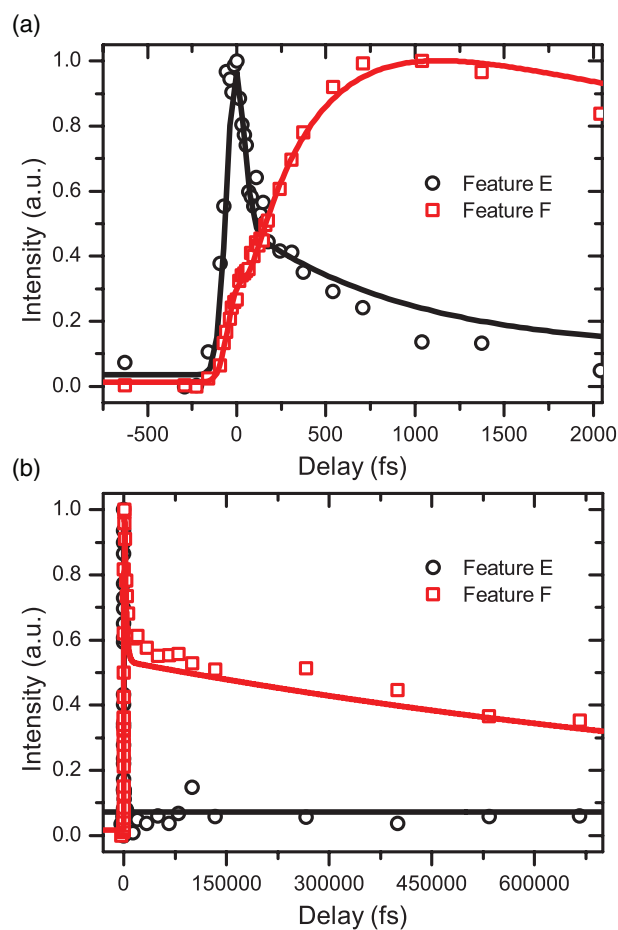


FIG. 8. Integrated intensities of the transient features E and F observed in $\Gamma^- \cdot \text{CH}_3\text{NO}_2$ TRPE spectra pumped with 3.60 eV and probed at 1.56 eV. Panel (a) shows the initial decay of feature E (black circles) and the concomitant rise of feature F (red squares) near the zero of pump-probe delay, while panel (b) shows the long-time decay of the two features. Fits are displayed as solid lines.

and a molecular response function⁶⁰

$$M(t) = I_0 \quad t < 0, \\ I_0 + \sum_i A_i \exp\left(\frac{-t}{\tau_i}\right) \quad t \geq 0, \quad (4)$$

in which I_0 is the signal background, A_i are coefficients, τ_i are time constants, and the full width at half-maximum of the Gaussian function represents the cross correlation σ_{CC} of the pump and probe pulses. The integrated intensity of feature E in $\Gamma^- \cdot \text{CH}_3\text{NO}_2$ can be fit by a single exponential function, while features C for $\Gamma^- \cdot \text{CH}_3\text{CN}$ and F for $\Gamma^- \cdot \text{CH}_3\text{NO}_2$ require two exponential functions to describe their decay. Feature F requires an additional exponential function to capture its belated rise. To reduce the influence of the spectral overlap between features E and F, only the high energy side of the peak of feature E was examined in the fitting.

Table II summarizes the parameters used in the fittings at two excitation energies for each system. Fitted parameters were extracted from concatenate fitting of multiple data sets and do not exhibit any notable trends with excitation energy. For feature C of the $\Gamma^- \cdot \text{CH}_3\text{CN}$ system, average τ_1 and τ_2 values are 4.7 ps and 880 ps. Feature E of $\Gamma^- \cdot \text{CH}_3\text{NO}_2$ decays

TABLE II. Timescales describing integrated intensities of features C, E, and F for the $I^- \cdot CH_3CN$ and $I^- \cdot CH_3NO_2$ complexes.

$h\nu_1$ (eV)	Feature	τ_1 (ps)	τ_2 (ps)	τ_3 (ps)
$I^- \cdot CH_3CN$ complex				
3.47	C	3.4 ± 1.8	840 ± 140	
3.53	C	5.9 ± 1.8	920 ± 90	
$I^- \cdot CH_3NO_2$ complex				
3.55	E	0.63 ± 0.11		
	F	2.3 ± 0.2	1100 ± 200	0.37 ± 0.04
3.60	E	0.46 ± 0.06		
	F	2.4 ± 0.4	1300 ± 200	0.42 ± 0.05

with time constants in the range of 500 fs while decay time constants for feature F are near 2 ps and 1200 ps. The rise of feature F is described by τ_{3F} as approximately 400 fs.

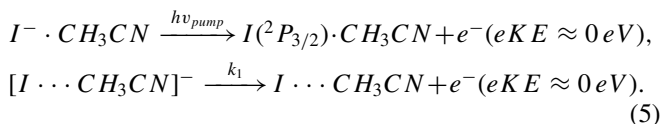
VI. DISCUSSION

UV excitation of an iodide-molecule complex in the range of the VDE of the complex according to Eq. (1) can be considered an electron scattering process wherein photodetachment of an electron from iodide can either produce a free electron and a neutral iodine-molecule complex or a transient negative ion of the form $[I \cdots M]^-$. The nature and decay of such TNIs has been explored experimentally using photoelectron and action spectroscopies for small solvent molecules^{25,39,61} and with TRPES for the nucleobases uracil and thymine.^{43,44} For acetonitrile and nitromethane, characterization of anionic photofragments suggests that the TNI represents the result of intracluster charge transfer from the iodide to the adjacent electropositive methyl groups of the associated molecules.^{25,39} In Secs. VI A–VI C, we consider the charge-transfer processes for these systems from a time-resolved perspective and explore the dynamics of their resultant TNIs in detail.

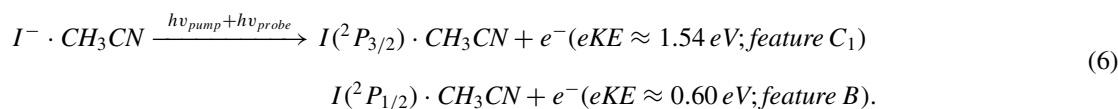
A. Dynamics of the iodide-acetonitrile complex

In the time-resolved photoelectron spectra of the photoexcited $I^- \cdot CH_3CN$ complex, feature A occurs at low eKE

and displays minimal temporal evolution. Because the excitation energies used are close in value to the VDE of the initial complex, direct single-photon detachment of $I^- \cdot CH_3CN$ should contribute to this low energy signal via production of the $I(^2P_{3/2}) \cdot CH_3CN$ neutral complex and a slow free electron. Electron autodetachment from the metastable TNI or other species can also produce low energy electron signal. Thus, the processes contributing to feature A can be summarized by the following equation:



In contrast to feature A, features B and C_1 exhibit notable dependence on excitation energy and pump-probe delay. As shown in Figures 3(a) and 4, these features appear as Gaussian peaks with widths reflective of the cross-correlation of the pump and probe pulses, indicating that both pulses contribute to the respective photoelectron signals. Feature C_1 becomes more intense relative to feature C_2 near the fringes of the photoabsorption spectrum of the DBS (Figure 5), appearing most dominant at energies furthest from the VDE of the initial complex, 3.54 eV.²⁵ Moreover, as shown in Figure 6, the eKE of feature C_1 tracks the pump photon energy, in contrast to feature C_2 which remains fixed. These observations suggest that feature C_1 is only weakly associated with the absorption resonance, if at all. The position and intensity of feature B in the time-resolved photoelectron spectra reflects the same trends as feature C_1 as it always occurs at about 0.9 eV higher electron binding energy than feature C_1 . This energy difference corresponds to the spin-orbit splitting of iodine, suggesting that features B and C_1 arise from photodetachment of a species with the electronic character of iodide as opposed to an excited charge-transfer complex. Thus, features B and C_1 are assigned to two-photon, two-color photodetachment (2CPD) of the initial $I^- \cdot CH_3CN$ complex, a channel unavailable outside of the overlap of the two pulses. Indeed, the central eKE of feature C_1 is consistent with that expected for 2CPD of the complex to yield iodine ($^2P_{3/2}$)-acetonitrile, while feature B is consistent with the formation of iodine ($^2P_{1/2}$)-acetonitrile:



The anisotropy parameters for feature C_1 are consistent with the assignment of the cross-correlation limited features to 2CPD (Figure 7(a)). The near-zero value of β_2 measured at $\Delta t = 0$ differs from the value of approximately -0.6 expected for single-photon detachment of both bare iodide and the iodide-acetonitrile complex.⁶² However, the non-zero value of β_4 at $\Delta t = 0$ and the corresponding photoelectron angular distribution displayed in Figure 2(a) indicate a multiphoton process.⁶³

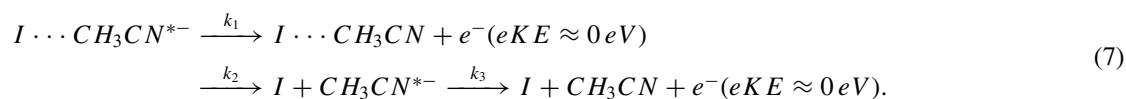
The transient negative ion $[I \cdots CH_3CN]^-$ created upon photoexcitation of $I^- \cdot CH_3CN$ represents the result of intracluster charge transfer from iodide to the acetonitrile molecule. In previous studies,^{25,64} this state was described as a dipole-bound acetonitrile anion perturbed by an iodine atom. The dipole-bound anion of bare acetonitrile has an electron binding energy smaller than 20 meV^{22,24,25} and produces a sharply peaked photoelectron signal.²⁵ Iodine is

expected to minimally perturb the acetonitrile DBS, and the binding energy of neutral iodine to molecules and cluster anions has been estimated as approximately 50 meV.^{59,65–68} Thus, the narrow and weakly bound (VDE = 20 meV) feature C₂ can reasonably be assigned to direct photodetachment of the dipole-bound acetonitrile anion by the probe pulse. The asymptotic anisotropy values depicted in Figure 7(a) also support this assignment, as the β_2 value of unity matches previously reported values⁶⁹ while the β_4 value of zero is consistent with single-photon photodetachment. β_2 values near unity are expected for dipole-bound electrons, which are generally well-described by hybrid *s-p_z* orbitals with predominantly *s* character.^{70,71}

As discussed above, the intensity of feature C₂ decays biexponentially with time constants of few and hundreds of ps. Because the dipole-bound state is so weakly bound, autodetachment of low energy electrons according to Eq. (5) should be facile if the TNI is formed with any vibrational excitation. The biexponential behavior observed is characteristic of a sequential process, however, indicating that other processes must also be considered. The TNI created upon charge transfer from iodide to acetonitrile should consist of an iodine atom complexed to the methyl end of a weakly excited dipole-bound acetonitrile anion, and can be described as $I \cdots CH_3CN^{*-}$. Only a small amount of energy should be available to the DBS because the excitation energy is close to the VDE of the initial complex. Thus, dissociation of the C–C bond to produce cyanide and a methyl radical or of a C–H bond to form a proton or hydrogen atom and a singly or

doubly charged allene-like H_2C_2N anion should not occur.^{72,73} The most viable decay pathway is thus iodine atom loss to yield the bare CH_3CN^{*-} DBS. With some excess energy carried away in translation by the departing iodine atom, the remaining CH_3CN^{*-} species should be further stabilized with respect to autodetachment and its rate of autodetachment should decrease.

Iodine loss has previously been invoked to explain biexponential decay of the transient negative ions of iodine-complexed uracil and thymine^{43,44} and has been hypothesized to occur for $I^- \cdot (CH_3CN)_n$ complexes with $n \geq 1$. For example, in a TRPES study of $n = 5–10$ clusters, a 50 meV drop in the cluster anion species' VDE was interpreted as the loss of iodine to yield the bare cluster anions.⁷⁴ Johnson and co-workers²⁵ noted the exclusive production of CH_3CN^- upon excitation of the $I^- \cdot CH_3CN$ binary complex near its VDE, suggesting that iodine is ineffective at electron recapture. Theoretical studies^{59,75} have also cited iodine loss as a process accompanying or subsequent to cluster rearrangements; a recent *ab initio* study by Mak *et al.*⁵⁹ indicated that a translation of iodine by several Å away from the acetonitrile moiety dominates the early dynamics of the photoexcited $n = 1$ cluster and reduces the VDE of the anion by less than 10 meV, a change difficult to observe in our experiment. Similarly, Takayanagi⁷⁵ used high level calculations to show that iodine translation away from the asymmetric, linear $n = 2$ cluster occurs with minimal change in VDE over hundreds of femtoseconds. The decay dynamics proposed for photo-excited $I^- \cdot CH_3CN$ are summarized in Eq. (7):



Within this scheme, the time constants can be related to rate constants according to

$$\tau_1 = \frac{1}{k_1 + k_2} \quad \tau_2 = \frac{1}{k_3}. \tag{8}$$

The autodetachment rate for the unperturbed DBS is given by $k_3 \sim 1 \times 10^9/s$. The autodetachment rate k_1 of the $I \cdots CH_3CN^{*-}$ state is difficult to disentangle from the rate of iodine loss. However, given that $k_1 + k_2 \sim 2 \times 10^{11}/s \gg k_3$, we would expect that $k_1 \ll k_2$ unless loss of iodine reduces the autodetachment rate by two orders of magnitude, which seems unlikely.

B. Dynamics of the iodide-nitromethane complex

The time-resolved photoelectron spectra for $I^- \cdot CH_3NO_2$ differ significantly from those for $I^- \cdot CH_3CN$ (Figure 3). While spectra for both systems include an intense low energy feature and a feature with eKE comparable to the energy of the probe pulse, feature C observed for $I^- \cdot CH_3CN$ persists for hundreds of ps while feature E appears to rapidly decay to

the much broader feature F in $I^- \cdot CH_3NO_2$ spectra. As discussed below, this divergence is attributable to a DBS to VBS transition in the nitromethane system that is not accessible for acetonitrile.

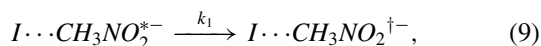
The time-resolved photoelectron spectra of the $I^- \cdot CH_3NO_2$ complex are dominated by a low eKE, near-time-invariant feature D. Direct detachment of the initial complex by the exciting pulse and autodetachment from the weakly bound transient negative ion state should both contribute to this photoelectron signal according to Eq. (5). In contrast to the $I^- \cdot CH_3CN$ system, two photon, two-color photodetachment of $I^- \cdot CH_3NO_2$ at the overlap of the pump and probe pulses is only weakly observed.

Intracluster charge transfer from the iodide to the nitromethane moiety initiated with a UV pulse close in energy to the VDE of the initial complex has previously been observed to produce a nitromethane anion with dipole-bound character, as inferred from the comparison of field-stripping measurements³⁹ with previous work on known dipole-bound states.^{16,23} The eBE of the nitromethane DBS was measured to be approximately 10 meV in RET¹⁶ and PES³⁴

experiments; interaction between the nitromethane anion and a neutral iodine atom may somewhat increase the VDE of the TNI complex.^{16,39,65–68} The narrow feature E with its VDE of approximately 20 meV is consistent with this description and is therefore identified as the DBS of nitromethane. The positive value of the associated β_2 anisotropy parameter supports the assignment of this feature as described in Sec. VI A.

The overall structure and spectral extent (0.3–1.5 eV eKE) of feature F are characteristic of a valence-bound anion for which large deviations between neutral and anion geometries produce broad Franck-Condon envelopes. In previous single-photon photoelectron spectroscopy measurements,^{16,33,34} the valence anion of nitromethane was generated in supersonic expansions of argon gas and its VDE and onset estimated to occur at 0.9 eV and 172 meV, respectively. Associated β_2 values were measured in the range of 0.5–1.25,^{33,34} consistent with detachment from the a' highest occupied molecular orbital of nitromethane.^{33,37} The energetic and anisotropy parameters observed for feature F match those previously reported and therefore support the assignment of F as the VBS of nitromethane. Here, no vibrational structure is observed, reflecting our energy resolution and the expectation that the valence anions have non-negligible vibrational excitation, leading to a spectrally congested spectrum.

The rapid decay of the DBS and coincident rise of the VBS implies that transformation to the VBS is the primary decay mechanism of the dipole-bound anion. The time constants τ_{1E} and τ_{3F} describing the decay of feature E and the rise of feature F, respectively, are roughly equivalent in value; the slightly larger values of τ_{1E} most likely result from residual contamination of feature E by feature F. As discussed for the acetonitrile anion, autodetachment and iodine atom loss could possibly also contribute to the initial decay of the iodine-stabilized DB anion of nitromethane. However, given that the decay of feature E is best captured with a single-exponential decay constant that is approximately equal to the rise time of feature F, it appears that these other channels are unimportant for the nitromethane dipole-bound anion. Thus, the decay dynamics of feature E are given by



where $I \cdots CH_3NO_2^{\dagger-}$ represents the iodine-associated valence anion described by feature F.

The transformation from the DBS to the VBS will now be considered in greater detail. The rate of the transformation is given by the rise τ_{3F} of feature F as approximately 400 fs. To our knowledge, this represents the first measurement of the rate of transfer between two such states. The transition had previously been predicted to occur on a

sub-microsecond timescale based upon a calculated coupling element between the two states of 30 meV.¹⁷

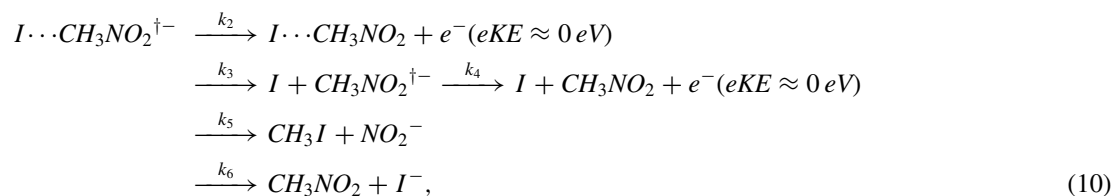
Figure 9 shows schematic diabatic potential energy curves for the relevant states.⁷⁶ The grey curve is neutral CH_3NO_2 , the blue curve is the anion DBS, which is slightly lower in energy relative to the neutral with a very similar geometry, and the red curve is the anion VBS, lying lower in energy than the DBS and exhibiting considerably more pyramidalization at the NO_2 group (see Table I). The transition from the DBS to the VBS must thus involve activation of the vibrational modes associated with the nitro group that dominate the photoelectron spectra of the VBS.^{16,34}

Figure 9 emphasizes the presumed role of the DBS as a Feshbach resonance and, consequently, a “doorway” into the valence anion state.^{16,17,37,39} The transition from the DBS should proceed upon vibrational energy redistribution^{35,76} into nitro group modes over a small barrier to produce a highly vibrationally excited valence anion. The height of this barrier has not been calculated, but RET studies measuring mixed dipole-valence character nitromethane anions suggest that it should be small.^{16,23,35} The limited previous observations of the DBS of nitromethane outside of RET experiments^{34,39} confirm the fragile nature of DBS emphasized by this scheme, as does the rapid DBS-VBS transition seen in the work presented here.

The highly vibrationally excited valence anion created upon this curve-crossing motion should be susceptible to decay via autodetachment and other mechanisms. The integrated intensity of the anion VBS exhibits clear biexponential behavior described by 2 ps and 1200 ps time constants. Notably, the spectral profile of feature F does not appear to change with Δt . As discussed above, the nature and rapidity of the DBS to VBS transformation suggests that the iodine remains associated with the nitromethane moiety during the transition. Hence, the same explanation proposed for the biexponential decay in $I^- \cdot CH_3CN$ (Eq. (7)) may well hold here.

Dissociation of the complex by loss of the nitrite ion or regeneration of the halide should also be considered. In action spectroscopy studies of bromide- and iodide-nitromethane complexes excited near their VDEs, Johnson and co-workers³⁹ noted the formation of both such species, invoking a radical-anion reaction to explain their formation with such small available energies.^{8,77–80} However, neither NO_2^- nor I^- can be detached at the probe photon energy used here,⁸¹ so the separate contribution of these channels to the decay of feature F cannot be assessed.

The dynamics describing the decay of the valence anion species are presented in Eq. (10):



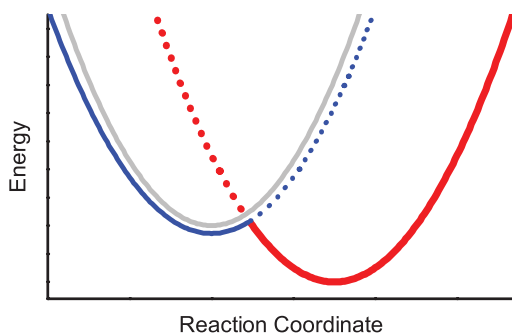


FIG. 9. Schematic of the potential energy surfaces involved in the transition from the dipole-bound state (blue curve) to the valence-bound state (bold red curve, lower right) of CH_3NO_2^- . The potential energy surface for neutral CH_3NO_2 is shown in gray.

in which $\text{CH}_3\text{NO}_2^{\dagger-}$ represents the relaxed valence anion and for which time constants are represented by

$$\tau_{1F} = \frac{1}{k_2 + k_3 + k_5 + k_6} \quad \tau_{2F} = \frac{1}{k_4}. \quad (11)$$

The autodetachment rate for the relaxed valence anion, τ_{2F} , is approximately $1 \times 10^9/\text{s}$, similar to that measured for the decay of the bare CH_3CN dipole-bound anion.

C. Comparison to iodide-nucleobase complexes

The experiments performed here were motivated by our earlier TRPES studies of iodide-uracil ($\text{I}^- \cdot \text{U}$) and iodide-thymine ($\text{I}^- \cdot \text{T}$) complexes.^{43,44} In those experiments, the complexes were excited approximately 0.7 eV above their respective VDEs, with the goal of producing nucleobase transient negative ions and elucidating their decay dynamics. For both complexes, a single, broad transient feature resembling the valence anion was observed.^{43,44} TNIs for both species decayed biexponentially, with the rates of uracil anion decay being considerably slower than those describing the thymine anion. These dynamics were interpreted as autodetachment of the iodine-complexed and bare anions, respectively, using similar arguments as those proposed here for $\text{I}^- \cdot \text{CH}_3\text{CN}$ and $\text{I}^- \cdot \text{CH}_3\text{NO}_2$ complexes.

Nucleobases are known to support dipole bound anion states¹¹ and very close-lying valence bound states.^{45,46,82} However, in contrast to the work presented here, our early experiments on $\text{I}^- \cdot \text{U}$ and $\text{I}^- \cdot \text{T}$ showed no evidence for DBS formation even as a short-lived transient species. Moreover, the biexponential decays measured for $\text{I}^- \cdot \text{CH}_3\text{CN}$ and $\text{I}^- \cdot \text{CH}_3\text{NO}_2$ are noticeably slower than for the nucleobase complexes. These differences may simply reflect the higher pump photon energies relative to the VDE in the experiments on iodide-nucleobase complexes or something more fundamental to the relaxation of the various TNIs.

Excitation of iodide-nucleobase complexes closer to their VDEs may yield iodine-stabilized dipole-bound anions in analogy to the acetonitrile and nitromethane systems. If so, an intermediate excitation energy may exist at which both the DBS and the VBS could be observed. Such an observation could provide considerable insight into the interaction

of nucleobases with low energy electrons and may assist in the understanding of radiation-induced damage to larger biological systems.

VII. CONCLUSION

The decay dynamics of the acetonitrile and nitromethane dipole-bound anions created by UV-initiated charge transfer within the corresponding iodide-molecule complexes have been investigated using time-resolved photoelectron imaging. The ground-state acetonitrile anion exists as a dipole-bound species, and the formation of a valence anion is not anticipated below 3 eV. The acetonitrile DBS generated upon electron transfer from iodide decays biexponentially with timescales of 4 ps and 900 ps, corresponding to translation of the iodine atom away from the molecule and electron autodetachment from the bare DBS. For the nitromethane system, both dipole-bound and valence anions are observed. The fast (400 fs) rise of the valence species and biexponential decay over 2 ps and 1200 ps timescales are suggestive of a DBS to VBS transition mediated by vibrational energy redistribution from methyl- to nitro-associated vibrational modes. The highly vibrationally excited VBS subsequently decays via autodetachment, iodine atom loss, and other dissociation mechanisms. These measurements mark the first direct observation of the transformation of a dipole-bound anion to a valence anion and may provide insight into the interactions between similar states in more complex systems such as uracil and thymine nucleobases.

ACKNOWLEDGMENTS

The work described herein was funded by the National Science Foundation (NSF) under Grant No. CHE-1011819. M.A.Y. gratefully acknowledges support from an NSF Graduate Research Fellowship.

- ¹E. Fermi and E. Teller, *Phys. Rev.* **72**, 399 (1947).
- ²J. E. Turner, *Am. J. Phys.* **45**, 758 (1977).
- ³W. R. Garrett, *Chem. Phys. Lett.* **5**, 393 (1970).
- ⁴O. H. Crawford, *Mol. Phys.* **20**, 585 (1971).
- ⁵O. H. Crawford and W. R. Garrett, *J. Chem. Phys.* **66**, 4968 (1977).
- ⁶W. R. Garrett, *J. Chem. Phys.* **69**, 2621 (1978).
- ⁷W. R. Garrett, *J. Chem. Phys.* **77**, 3666 (1982).
- ⁸J. A. Stockdale, F. J. Davis, R. N. Compton, and C. E. Klots, *J. Chem. Phys.* **60**, 4279 (1974).
- ⁹R. Hashemi and E. Illenberger, *J. Phys. Chem.* **95**, 6402 (1991).
- ¹⁰H. Haberland, C. Ludewigt, H. G. Schindler, and D. R. Worsnop, *J. Chem. Phys.* **81**, 3742 (1984).
- ¹¹J. H. Hendricks, S. A. Lyapustina, H. L. deClercq, J. T. Snodgrass, and K. H. Bowen, *J. Chem. Phys.* **104**, 7788 (1996).
- ¹²C. Desfrancois, H. Abdoul-Carime, N. Khelifa, and J. P. Schermann, *Phys. Rev. Lett.* **73**, 2436 (1994).
- ¹³K. R. Lykke, D. M. Neumark, T. Andersen, V. J. Trapa, and W. C. Lineberger, *J. Chem. Phys.* **87**, 6842 (1987).
- ¹⁴E. A. Brinkman, S. Berger, J. Marks, and J. I. Brauman, *J. Chem. Phys.* **99**, 7586 (1993).
- ¹⁵K. R. Lykke, R. D. Mead, and W. C. Lineberger, *Phys. Rev. Lett.* **52**, 2221 (1984).
- ¹⁶R. N. Compton, J. H. S. Carman, C. Desfrancois, H. Abdoul-Carime, J. P. Schermann, J. H. Hendricks, S. A. Lyapustina, and K. H. Bowen, *J. Chem. Phys.* **105**, 3472 (1996).
- ¹⁷T. Sommerfeld, *Phys. Chem. Chem. Phys.* **4**, 2511 (2002).
- ¹⁸T. Sommerfeld, *J. Phys.: Conf. Ser.* **4**, 245 (2005).

- ¹⁹C. E. Klots, *J. Chem. Phys.* **62**, 741 (1975).
- ²⁰G. L. Gutsev, A. L. Sobolewski, and L. Adamowicz, *Chem. Phys.* **196**, 1 (1995).
- ²¹M. Gutowski, K. D. Jordan, and P. Skurski, *J. Phys. Chem. A* **102**, 2624 (1998).
- ²²C. Desfrancois, H. Abdoul-Carime, C. Adjouri, N. Khelifa, and J. P. Schermann, *Europhys. Lett.* **26**, 25 (1994).
- ²³F. Lecomte, S. Carles, C. Desfrancois, and M. A. Johnson, *J. Chem. Phys.* **113**, 10973 (2000).
- ²⁴R. A. Pople, C. D. Finch, and F. B. Dunning, *Chem. Phys. Lett.* **234**, 172 (1995).
- ²⁵C. E. H. Dessent, C. G. Bailey, and M. A. Johnson, *J. Chem. Phys.* **103**, 2006 (1995).
- ²⁶L. Suess, Y. Liu, R. Parthasarathy, and F. B. Dunning, *J. Chem. Phys.* **119**, 12890 (2003).
- ²⁷L. Suess, Y. Liu, R. Parthasarathy, and F. B. Dunning, *Chem. Phys. Lett.* **376**, 376 (2003).
- ²⁸M. Cannon, Y. Liu, L. Suess, and F. B. Dunning, *J. Chem. Phys.* **128**, 244307 (2008).
- ²⁹P. D. Burrow, A. E. Howard, A. R. Johnston, and K. D. Jordan, *J. Phys. Chem.* **96**, 7570 (1992).
- ³⁰F. Edard and M. Tronc, *J. Phys. B: At. Mol. Phys.* **20**, L265 (1987).
- ³¹R. N. Compton, P. W. Reinhardt, and C. D. Cooper, *J. Chem. Phys.* **68**, 4360 (1978).
- ³²P. R. Brooks, P. W. Harland, and C. E. Redden, *J. Am. Chem. Soc.* **128**, 4773 (2006).
- ³³D. J. Goebbert, K. Pichugin, and A. Sanov, *J. Chem. Phys.* **131**, 164308 (2009).
- ³⁴C. L. Adams, H. Schneider, K. M. Ervin, and J. M. Weber, *J. Chem. Phys.* **130**, 074307 (2009).
- ³⁵J. M. Weber, W. H. Robertson, and M. A. Johnson, *J. Chem. Phys.* **115**, 10718 (2001).
- ³⁶H. Schneider, K. M. Vogelhuber, F. Schinle, J. F. Stanton, and J. M. Weber, *J. Phys. Chem. A* **112**, 7498 (2008).
- ³⁷G. L. Gutsev and R. J. Bartlett, *J. Chem. Phys.* **105**, 8785 (1996).
- ³⁸S. T. Stokes, K. H. Bowen, T. Sommerfeld, S. Ard, N. Mirsaleh-Kohan, J. D. Steill, and R. N. Compton, *J. Chem. Phys.* **129**, 064308 (2008).
- ³⁹C. E. H. Dessent, J. Kim, and M. A. Johnson, *Faraday Discuss.* **115**, 395 (2000).
- ⁴⁰F. Mbaïwa, D. Dao, N. Holtgrewe, J. Lasinski, and R. Mabbs, *J. Chem. Phys.* **136**, 114303 (2012).
- ⁴¹O. T. Ehrler and D. M. Neumark, *Acc. Chem. Res.* **42**, 769 (2009).
- ⁴²R. M. Young and D. M. Neumark, *Chem. Rev.* **112**, 5553 (2012).
- ⁴³M. A. Yandell, S. B. King, and D. M. Neumark, *J. Am. Chem. Soc.* **135**, 2128 (2013).
- ⁴⁴S. B. King, M. A. Yandell, and D. M. Neumark, *Faraday Discuss.* **163**, 59 (2013).
- ⁴⁵J. H. Hendricks, S. A. Lyapustina, H. L. de Clercq, and K. H. Bowen, *J. Chem. Phys.* **108**, 8 (1998).
- ⁴⁶J. Schiedt, R. Weinkauff, D. M. Neumark, and E. W. Schlag, *Chem. Phys.* **239**, 511 (1998).
- ⁴⁷A. V. Davis, R. Wester, A. E. Bragg, and D. M. Neumark, *J. Chem. Phys.* **118**, 999 (2003).
- ⁴⁸A. E. Bragg, J. R. R. Verlet, A. Kammrath, O. Cheshnovsky, and D. M. Neumark, *J. Am. Chem. Soc.* **127**, 15283 (2005).
- ⁴⁹M. A. Yandell, R. M. Young, S. B. King, and D. M. Neumark, *J. Phys. Chem. A* **116**, 2750 (2012).
- ⁵⁰U. Even, J. Jortner, D. Noy, N. Lavie, and C. Cossart-Magos, *J. Chem. Phys.* **112**, 8068 (2000).
- ⁵¹W. C. Wiley and I. H. McLaren, *Rev. Sci. Instrum.* **26**, 1150 (1955).
- ⁵²V. Dribinski, A. Ossadtchi, V. A. Mandelshtam, and H. Reisler, *Rev. Sci. Instrum.* **73**, 2634 (2002).
- ⁵³G. M. Roberts, J. L. Nixon, J. Lecointre, E. Wrede, and J. R. R. Verlet, *Rev. Sci. Instrum.* **80**, 053104 (2009).
- ⁵⁴K. L. Reid, *Annu. Rev. Phys. Chem.* **54**, 397 (2003).
- ⁵⁵M. J. Frisch, G. W. Trucks, H. B. Schlegel *et al.*, Gaussian 09, Revision B.01, Gaussian, Inc., Wallingford, CT, 2009.
- ⁵⁶K. A. Peterson, B. C. Shepler, D. Figgen, and H. Stoll, *J. Phys. Chem. A* **110**, 13877 (2006).
- ⁵⁷Q. K. Timerghazin and G. H. Peslherbe, *Chem. Phys. Lett.* **354**, 31 (2002).
- ⁵⁸T.-N. V. Nguyen and G. H. Peslherbe, *J. Phys. Chem. A* **107**, 1540 (2003).
- ⁵⁹C. C. Mak, Q. K. Timerghazin, and G. H. Peslherbe, *J. Phys. Chem. A* **117**, 7595 (2013).
- ⁶⁰S. Pedersen and A. H. Zewail, *Mol. Phys.* **89**, 1455 (1996).
- ⁶¹C. E. H. Dessent, C. G. Bailey, and M. A. Johnson, *J. Chem. Phys.* **102**, 6335 (1995).
- ⁶²R. Mabbs, E. Surber, and A. Sanov, *J. Chem. Phys.* **122**, 054308 (2005).
- ⁶³S. Tauro and K. Liu, *J. Phys. B: At., Mol. Opt. Phys.* **41**, 225001 (2008).
- ⁶⁴C. G. Bailey, C. E. H. Dessent, M. A. Johnson, and J. Kit H. Bowen, *J. Chem. Phys.* **104**, 6976 (1996).
- ⁶⁵H. Y. Chen and W. S. Sheu, *Chem. Phys. Lett.* **335**, 475 (2001).
- ⁶⁶A. Kammrath, J. R. R. Verlet, A. E. Bragg, G. B. Griffin, and D. M. Neumark, *J. Phys. Chem. A* **109**, 11475 (2005).
- ⁶⁷C. C. Mak, Q. K. Timerghazin, and G. H. Peslherbe, *Phys. Chem. Chem. Phys.* **14**, 6257 (2012).
- ⁶⁸W.-S. Sheu and M.-F. Chiou, *J. Phys. Chem. A* **117**, 13946 (2013).
- ⁶⁹F. Mbaïwa, Ph.D. dissertation (Washington University, St. Louis, 2011).
- ⁷⁰C. Desfrancois, H. Abdoul-Carime, and J.-P. Schermann, *Int. J. Mod. Phys. B* **10**, 1339 (1996).
- ⁷¹R. Mabbs, E. R. Grumblin, K. Pichugin, and A. Sanov, *Chem. Soc. Rev.* **38**, 2169 (2009).
- ⁷²W. Sailer, A. Pelc, P. Limão-Vieira, N. J. Mason, J. Limtrakul, P. Scheier, M. Probst, and T. D. Märk, *Chem. Phys. Lett.* **381**, 216 (2003).
- ⁷³M. Heni and E. Illenberger, *Int. J. Mass Spectrom. Ion Processes* **73**, 127 (1986).
- ⁷⁴O. T. Ehrler, G. B. Griffin, R. M. Young, and D. M. Neumark, *J. Phys. Chem. B* **113**, 4031 (2009).
- ⁷⁵T. Takayanagi, *J. Phys. Chem. A* **110**, 7011 (2006).
- ⁷⁶C. L. Adams, H. Schneider, and J. M. Weber, *J. Phys. Chem. A* **114**, 4017 (2010).
- ⁷⁷W. Sailer, A. Pelc, S. Matejcik, E. Illenberger, P. Scheier, and T. D. Märk, *J. Chem. Phys.* **117**, 7989 (2002).
- ⁷⁸J. F. Arenas, J. C. Otero, D. Peláez, J. Soto, and L. Serrano-Andrés, *J. Chem. Phys.* **121**, 4127 (2004).
- ⁷⁹E. Alizadeh, F. Ferreira da Silva, F. Zappa, A. Mauracher, M. Probst, S. Denifl, A. Bacher, T. D. Märk, P. Limão-Vieira, and P. Scheier, *Int. J. Mass Spectrom.* **271**, 15 (2008).
- ⁸⁰D. J. Goebbert, D. Khuseynov, and A. Sanov, *J. Chem. Phys.* **133**, 084311 (2010).
- ⁸¹K. M. Ervin, J. Ho, and W. C. Lineberger, *J. Phys. Chem.* **92**, 5405 (1988).
- ⁸²J. Gu, J. Leszczynski, and H. F. Schaefer, *Chem. Rev.* **112**, 5603 (2012).